Computing interacting multi-fronts in one dimensional Real Ginzburg Landau Equations

Tasos Rossides[1], David J.B. Lloyd[1], and Sergey Zelik[1]

[1]Department of Mathematics, University of Surrey, Guildford, GU2 7XH, UK

August 31, 2014

Abstract

We develop an efficient and robust numerical scheme to compute multi-fronts in one-dimensional Real Ginzburg-Landau equations that range from well-separated to strongly interacting and colliding. The scheme is based on the global centre-manifold reduction where one considers an initial sum of fronts plus a remainder function (not necessarily small) and applying a suitable projection based on the neutral Eigenmodes of each front. Such a scheme efficiently captures the weakly interacting tails of the fronts. Furthermore, as the fronts become strongly interacting, we show how they may be added to the remainder function to accurately compute through collisions. We then present results of our numerical scheme applied to various real Ginzburg Landau equations where we observe colliding fronts, travelling fronts and fronts converging to bound states. Finally, we discuss how this numerical scheme can be extended to general PDE systems and other multi-localised structures.

1 Introduction

Localised structures, such as fronts or pulses, appear in a range of physical situations from pulse propagation of impulses in nerve fibers in mathematical biology, to modelling pulse propagations in optical fibers, and weather fronts [1, 12]; see Figure 1 (a) and (b) for examples of fronts and backs where the "marker quantity" $u(x)$ connects two different quiescent states in space x. Frequently, such localised structures appear together (called multi-pulses or multi-fronts[1]) where one expects the fronts to interact with each other via their exponentially decaying tails inducing and influencing the movement of the fronts; see Figure 1 (c) for an example of a multi-front/back solution. The development of fast, efficient and robust numerical algorithms for a one-dimensional pulse/front has been largely resolved. A common approach (as implemented in the software package AUTO and HOMCONT [4]) is to find approximations of a pulse/front on a large but bounded domain and solve a two-point boundary value problem with projection boundary conditions [19]. Various standard methods for solving the two-point boundary value problem such as shooting, or orthogonal collocation can then be used to yield highly accurate solutions [2]. This approach has been used on a variety of different problems in order to use path-following routines to explore the bifurcation structure of pulses/fronts; see for example [4] and references therein.

The computation of well-separated multiple pulses or fronts remains a very challenging numerical problem due to the interaction of the tails of the pulses/fronts being exponentially small in the separation distance. In particular, the dynamics of weakly interacting pulses/fronts are known to have highly intricate structures that require very accurate numerics in order to capture them; see for example [1, 18, 26]. Several advances in the numerical computation of stationary one-dimensional multi-pulses have been made in ODEs. One approach to address this problem has been to use Lin's method to set-up a boundary value problem where

[1]Throughout this paper we will use the terms front and kink interchangeably and similarly for back and anti-kink.

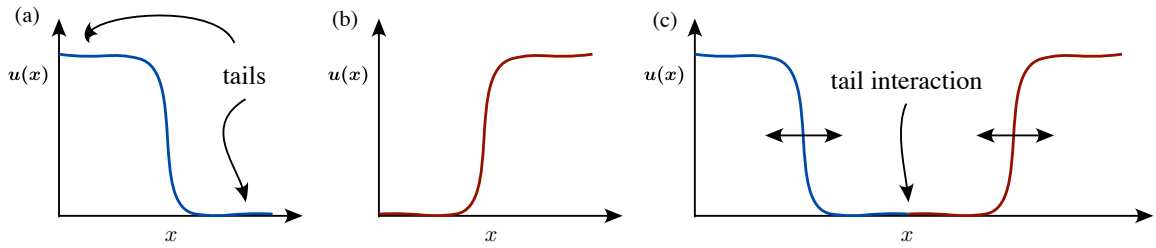

Figure 1: ***(a)*** *Localised structures anti-kink (back),* ***(b)*** *a kink (front) and* ***(c)*** *a multi-kink solution showing the interaction of the fronts via their tails.*

one looks for zeros of an algebraic function using path-following routines and has been implemented in HOMCONT; see [16].

For time-dependent well separated multi-pulses/fronts in PDEs, a standard scheme is to consider the linear combination of several single translated pulses/fronts and apply a projection based on the neutral modes of each translated pulse/front [5, 8, 21]. This projection typically leads to a set of ODEs describing the location of each pulse/front allowing for very accurate computation of the interaction terms and high order ODE algorithms to be used. One may also look at the steady states of the resulting ODE system via the projection to understand the dependence of the multi-pulses/fronts with respect to parameters.

Several authors have looked at strongly interacting localised structures in ODEs/PDEs to understand the effect of collisions; see [3, 11, 15]. Typical strong-interaction dynamics observed from collisions range from repulsion, annihilation, scattering of pulses and the generation of new pulses; see [13, 14]. For strongly interacting localised structures the interaction between the states becomes $\mathcal{O}(1)$ and standard numerical algorithms (such as Crank-Nicholson, exponential time-stepping with spectral collocation, method of lines etc.) can be used to efficiently compute such collisions. However, these algorithms become inefficient when the localised structures become well-separated.

Our aim is to develop an efficient and robust numerical scheme for computing multi-fronts that allows us to simulate and track multi-front states where the fronts may range from well-separated to strongly-interacting and colliding. Our scheme is based on the Global centre-manifold reduction of Zelik et al. [27] (see also [6, 17, 20]) where they consider a linear combination of several well-separated fronts/pulses plus a remainder function and apply a suitable projection based on the neutral Eigenmodes of each front/pulse. This reduction is in the same spirit of Lin's method. The reduction leads to a fast-slow ODE/PDE system where the ODEs describe the evolution of the location of each well-separated front and the PDE describes the evolution of the remainder function. Such a system is found to have several nice numerical properties that allow us to quickly evolve large numbers of multi-fronts. As the fronts become strongly-interacting the ODE/PDE system becomes ill-posed since the original assumption of well-separated fronts breaks down. However, one can detect when the ODE/PDE system becomes ill-posed, stop the simulation and remove the locations of the strongly-interacting fronts from the ODE/PDE system while adding the colliding fronts to the remainder function and solving a new ODE/PDE system. Hence, we maintain the numerical advantages of the ODE/PDE system throughout the simulation.

In order to demonstrate how the numerical scheme works in practice, we apply it to several Real Ginzburg-Landau (RGL) equations where we investigate the numerical advantages of the scheme over a standard method of lines scheme. In particular, we consider a PDE of the form

$$u_t = u_{xx} + f(u), \quad x \in \mathbb{R}, \tag{1.1}$$

where $u = u(x,t)$ and $f \in C^2(\mathbb{R})$ is a non-linear function that satisfies

$$f(1) = f(-1) = 0, \ f'(\pm 1) < 0, \tag{1.2a}$$

$$\exists!\ \eta \in (-1,1)\ s.t.\ f(\eta) = 0, \text{ and,} \tag{1.2b}$$

$$f'(\eta) > 0. \tag{1.2c}$$

The kink profile $u(x,t) := V(\xi)$, where $\xi = ct - x$, when substituted in (1.1) solves

$$V_{\xi\xi} + cV_\xi + f(V) = 0, \quad V'(\xi) > 0, \quad \lim_{\xi \to \pm\infty} V(\xi) = \pm 1, \tag{1.3}$$

and both the velocity c and the profile V are uniquely determined by (1.3); see [25] for more details. In particular, this profile satisfies the identity

$$c \int_{-\infty}^{\infty} V'(\xi)^2 \, d\xi = F(-1) - F(+1),$$

where $F(z) := \int_0^z f(u)\, du$ is the antiderivative of f and this determines the direction of motion of the kink. The equation (1.1) also possesses an anti-kink (or back) solution that moves with the same velocity c, but in the opposite direction. We denote the kink/front solution as $u_+(x,t) = V(x - ct)$ and the anti-kink/back solution as $u_-(x,t) = V(-x - ct)$; see Figure 1 (a) & (b). Moreover, it also follows from the monotonicity of the kink ($V' > 0$) and Perron-Frobenius theory that the kink is locally stable; see [25] and references therein. In particular, the linearized operator

$$L_c := \partial_\xi^2 + c\partial_\xi + f'(V(\xi)),$$

considered as an unbounded operator in $L^2(\mathbb{R})$ with the domain $D = H^2(\mathbb{R})$ (see for example [9]), has a simple zero eigenvalue with the corresponding eigenvector $\varphi(\xi) := V'(\xi)$ and the rest of the spectrum is negative and separated from zero. The nonlinear stability of the kink $u_+(x,t)$ implies that, for any initial data $u_0(x)$ satisfying

$$\|u_0 - V\|_{L^\infty(\mathbb{R})} \leq \delta,$$

for sufficiently small $\delta > 0$, there exists $x_0 = x_0(u_0)$ such that the corresponding solution $u(x,t)$ satisfies

$$\|u(\cdot,t) - V(\cdot - ct - x_0)\|_{L^\infty(\mathbb{R})} \leq Ce^{-\alpha t},$$

for some positive constants C and α. In other words, the local dynamics of (1.1) near the kink $u_+(x,t)$ is normally hyperbolic. The kink possesses a one-dimensional *neutral* direction generated by $\varphi(x - ct)$ (corresponding to the spatial shifts of the kink) and is exponentially stable in the transversal directions, w, that satisfy $\langle w, \psi \rangle = 0$ where $\psi = \psi(\xi)$ is the adjoint eigenfunction of L_c and solves the following problem

$$L_c^* \psi = (\partial_\xi^2 - c\partial_\xi + f'(V(\xi)))\psi = 0, \quad \langle \varphi, \psi \rangle := \int_{-\infty}^{\infty} \varphi(\xi)\psi(\xi)\, d\xi = 1, \tag{1.4}$$

see [25], [27] and references therein for more details.

Analogously to the kink $u_+(x,t)$, the anti-kink $u_-(x,t)$ is also locally stable.

We will apply our methods to the following RGL type equations where f in (1.1) is defined as follows

RGL1: $f(u) = u - u^3$,

RGL2: $f(u) = u - u^3 + \epsilon(u^2 - 1)$,

RGL3: $f(u) = u - u^3 + \epsilon \cos(x/2)$.

The first case, RGL1, is the standard real Ginzburg-Landau equation that possesses an explicit single stationary front solution where multi-fronts attract one another leading to collisions and annihilations; see [17]. RGL2 has an explicit travelling front solution where the fronts either attract or repel one another with collisions leading to annihilation for $\epsilon < 1$. For $\epsilon > 1$, the spatially homogeneous state $u = +1$ becomes unstable where it is not known how multi-fronts evolve and we will investigate this region of parameter space. The third equation, RGL3, possesses bound state fronts where it is possible that annihilation of fronts do not occur, depending on the initial conditions.

We study the weak interaction in *multi-kink* structures governed by equation (1.1) starting from the initial data

$$u_0(x) = V_{\Sigma_0}(x) + w_0(x) := \left[\sum_{i=1}^{n} V\left((-1)^i(x - d_i(0))\right) + h(n)\right] + w_0(x), \quad h(n) := \frac{1 + (-1)^n}{2}, \tag{1.5}$$

where $n \in \mathbb{N}$ and $d_1(0) < d_2(0) < \cdots < d_n(0)$ are the initial positions of the kinks/anti-kinks (assumed be well-separated, i.e., $d_{i+1}(0) - d_i(0) \gg 1$) and w_0 is a small remainder, say, in the $L^\infty(\mathbb{R})$ norm. The corrector $h(n)$ is necessary here in order to guarantee that multi-front structure V_{Σ_0} from (1.5) satisfies the assumption

$$\lim_{x \to \pm\infty} V_{\Sigma_0}(x) = \pm 1.$$

We seek the solution of (1.1) started from (1.5) in the following natural form:

$$u(x,t) := V_\Sigma(x,t) + w(x,t) = \sum_{i=1}^{n} V\left((-1)^i(x - d_i(t)) - ct\right) + h(n) + w(x,t), \tag{1.6}$$

where the functions $D_i(t) := d_i(t) - (-1)^i ct$ describe the evolution of the kink/anti-kink positions at time t, the remainder $w(x,t)$ remains small (again, say, in the $L^\infty(\mathbb{R})$ norm) and the time derivatives $d_i'(t)$ are also small due to the assumption that fronts are well-separated. Thus, (1.6) describes the so-called *weak* interaction of kink/antikinks and the limit case $w = 0$ formally corresponds to the non-interacting kinks.

It is well-known, see [6, 17, 20, 27], that the solution $u(x,t)$ in the form (1.6) exists indeed for all times $t \geq 0$ such that well-separation condition

$$\min_{1 \leq i \leq n-1} \{|D_{i+1}(s) - D_i(s)|\} > \Gamma \gg 1, \quad 0 \leq s \leq t, \quad \Gamma \in \mathbb{R}. \tag{1.7}$$

Moreover, there exists an n-dimensional invariant center manifold over the base

$$B_\Gamma := \{D \in \mathbb{R}^n, \ \min_{1 \leq i \leq n-1} \{|D_{i+1} - D_i|\} > \Gamma\}, \qquad D(t) := (D_1(t), \cdots, D_n(t)),$$

which consist of such solutions and any other solution starting from the small neighborhood of the manifold approaches the manifold exponentially fast. Thus, the dynamics of interacting well-separated kinks is finite-dimensional and can be described by the evolution of the kink positions $D(t) := (D_1(t), \cdots, D_n(t))$. Following the general centre manifold reduction scheme, we derive the system of ODEs describing the evolution of the kink positions D_i coupled to a PDE that describes the fast evolution of the remainder $w(x,t)$; see §2.2. The coupled ODE/PDE system described will be used for the high precision numerical simulations.

If fronts become too close together, the multi-kink structure (1.6) breaks down and the corresponding fronts collide, see e.g., [17]. We show how to monitor the break down and stop at an appropriate point where a new multi-kink structure (1.6) can be computed with w now including the colliding kinks. A major difficulty is that w needs to be orthogonal to the adjoint eigenfunctions of the remaining well-separated kinks and we show how one can overcome this difficulty to yield a new reduced ODE/PDE system to evolve.

Crucial to the numerical scheme working is the accurate computation of a single front/back and its neutral Eigenfunction such that the projected ODE/PDE system may correctly capture the weakly interacting tails of the fronts. We show how to overcome this problem and control all the errors of the simulation to an absolute error of approximately standard machine precession. Finally, we describe how this numerical scheme may be applied to other multi-localised states and PDE systems.

The paper is outlined as follows. In §2 we give an overview of the standard time stepping scheme (SS) and projected system scheme (PS) that will use and compare for evolving multi-kinks in three RGL-type equations. In §3 we present our numerical results and comparison of the two schemes. Finally, in §4 we draw conclusions and outline extensions of the projected system to other PDE systems.

2 Numerical Method

In this section we describe the numerical schemes we will use to evolve multi-fronts solutions of (1.1) and carry out a comparison and validation of our projection scheme. The first scheme describes how we evolve (1.1) with a standard method-of-lines scheme which we call a Standard time stepping Scheme (SS). The second scheme we present is the Projection Scheme (PS) based on the Global centre-manifold reduction of Zelik & Mielke [27].

To this end, we first introduce some notations and define the following

$$V_i = V_i(x,t) := V((-1)^i(x - d_i(t)) - ct), \tag{2.1}$$
$$\varphi_i = \varphi_i(x,t) := \partial_x V_i = (-1)^i V'((-1)^i(x - d_i(t)) - ct), \tag{2.2}$$
$$\psi_i = \psi_i(x,t) := (-1)^i \psi((-1)^i(x - d_i(t)) - ct). \tag{2.3}$$

2.1 Standard time stepping (SS) Scheme and retrieving the kink positions

In this section we explain how we employ a method-of-lines approach to simulating (1.1) with initial condition (1.5). First, we truncate the spatial domain from the real line to $x \in [0,\ L_x]$ where L_x is some large number and we apply homogeneous Neumann boundary conditions

$$u_x(0) = u_x(L_x) = 0.$$

Since the multi-front solution exists on the real line an error occurs due to this finite domain and boundary conditions. However, it can be shown that the error will decay exponentially in the truncation parameter L_x; see [19].

We discretise space $x^i = i\Delta x,\ i = 0, 1, \ldots, N_x$ where $\Delta x = 1/N_x$ is the spatial step size and $N_x + 1$ is the number of spatial mesh points. We approximate $u(x,t)$ with $u^i(t)$ and the second spatial derivative is approximated on the spatial mesh with 4th order finite-differences i.e.

$$u_{xx}(x^i) \approx \nabla^4 u^i(t) = \frac{-u^{i-2}(t) + 16u^{i-1}(t) - 30u^i(t) + 16u^{i+1}(t) - u^{i+2}(t)}{12\Delta x^2}. \tag{2.4}$$

The boundary conditions are imposed using ghost points; see [24] and setting $u^{-2} = u^2, u^{-1} = u^1, u^{N_x+1} = u^{N_x-1}$, and $u^{N_x+2} = u^{Nx-2}$. This discretisation yields a large system of stiff ODEs to evolve of the form $u_t^i = \nabla^4 u^i + f(u^i),\ i = 0, 1, \ldots, N_x$ with initial condition evaluated at the spatial mesh points. In order to time evolve the stiff ODE system we employ a variable order, adaptive time stepping method as implemented in MATLAB's `ode15s` ODE solver; see [22, 23]. We choose to use MATLAB's `ode15s` ODE solver for several reasons. Firstly, the solver allows for stringent error tolerances to be maintained throughout the simulation. Secondly, due to the multi-time-scale nature of the multi-kink interaction (slow movement of well-separated kinks verses fast movement of strongly interacting kinks), we believe that an adaptive time-stepping method will be significantly more efficient than a fixed time-stepping scheme. Thirdly, `ode15s` allows for event detection e.g., front collision that we will exploit in our simulations.

We will now briefly describe the algorithm that is implemented in MATLAB's ODE solver `ode15s`. Given an ODE system of the form $u' = f(u,t)$, `ode15s` computes a time-step u_{n+1} by solving the algebraic system defined by the Numerical Differentiation Formula [22, 23]

$$\sum_{m=1}^{k} \gamma_m \nabla^m u_n + (1-\kappa)\gamma_k(u_{n+1} - u_{n+1}^{[0]}) - hf(u_{n+1}, t_{n+1}) = 0,$$

for u_{n+1} using a simplified Newton (chord) method with the initial value $u_{n+1}^{[0]} = \sum_{m=0}^{k} \nabla^m u_n$, where k is the order of the scheme i.e. $k = 1, 2, 3, 4$ or 5, $\gamma_m = \sum_{j=1}^{m} \frac{1}{j}$, ∇^m is the m-th order finite-difference operator, κ is chosen optimally to maintain stability while maximising the time-step and h is the time-step size. In order to speed up the computation of the time-steps, we supply the analytical Jacobian for the righthand-side

of the ODE system. More details about the MATLAB solver and methods used for both schemes can be found in [10, 22].

Once the profile $u(x,t)$ is obtained, we still need to retrieve the kink/antikink positions $D_i(t)$ from it; see formula (1.6). Note however that there are in general many ways to present the solution $u(x,t)$ in the form (1.6) and we need to put extra conditions on the remainder w in order define the positions D_i in a unique way. Following the general scheme suggested in [27], we fix these extra assumptions in the form of the orthogonality conditions to the cokernel elements of the corresponding kinks i.e.,

$$\langle w, \psi_j \rangle = \left\langle u(\cdot,t) - \sum_{i=1}^{n} V_i - h(n), \psi_j \right\rangle = 0, \quad j = 1, \cdots, n, \tag{2.5}$$

where $h(n)$ is defined in (1.5), u is the numerical approximation of (1.1). Equations (2.5) give a system of n equations for the unknown kink positions $D_i = D_i(t)$ to be determined at every time t. The Jacobi matrix G of this system has the following entries:

$$G_{ij}(D,w) = \langle \varphi_i, \varphi_j \rangle + \delta_{ij} \langle w, \partial_{x_j} \psi_j \rangle, \quad w := u - \sum_{i=1}^{n} V_i - h(n), \tag{2.6}$$

where δ_{ij} is a Kronecker delta, and we can see that this matrix is close to the identity if D_j are well separated (see (1.7)) and w is small enough. Here we have implicitly used due to the non-degeneracy assumption $f'(\pm 1) \neq 0$, and

$$|\varphi(z)| + |\psi(z)| \leq Ce^{-\alpha|z|}, \ z \in \mathbb{R} \tag{2.7}$$

for some positive C and α and by this reason, if the distances D_j are large enough, the integrals $\langle \varphi_i, \psi_j \rangle$ are close to zero for $i \neq j$ (exponentially with respect to the distance between kinks). Thus, system (2.5) is indeed uniquely solvable if the profile $u(x,t)$ is close to the multi-kink profile (1.6) and the kink positions D_j are uniquelly defined by the profile u. We use the Newton's algorithm to solve this system numerically at each time-step and use the kink positions D_j found on the previous discrete time step as initial approximations for the next time step. We note that one can also just compute the kink positions D_j at a single time-step by making a sensible guess of the kink positions.

This method of tracking the fronts positions is simple, fast and is done "post-process" so as to not slow down the SS (we do not include the additional computational time for computing the kink positions in our wall-time comparisons in §3.2). Thus, after fixing the extra orthogonality conditions on the remainder w, the kink positions $D_i(t)$ indeed can be retrieved in a unique way from the solution profile $u(x,t)$ if the kinks are well-separated. We note that in the case of strongly interacting (colliding) kinks the above retrieving procedure may fail since the determinant of the Jacobi matrix G may become zero.

2.2 Projection system (PS)

In this section we will describe the projection scheme for computing multi-fronts in (1.1). The relevant stability conditions of the front in order to derive the projection system are stated in (1.2). Due to the normalization condition on kernel element φ and co-kernel element ψ, we find for φ_i and ψ_i

$$\langle \varphi_i, \psi_i \rangle = \int_R \varphi_i \psi_i \, dx = 1 \text{ for all } t \in \mathbb{R}, \tag{2.8}$$

and since the adjoint function ψ solves equation (1.4), the functions $\psi_i(x,t)$ solve

$$-\partial_t \psi_i = \partial_{xx} \psi_i + f'(V_i)\psi_i - \partial_x \psi_i d_i'. \tag{2.9}$$

We seek a solution of (1.1) of the form

$$u(x,t) = V_\Sigma(x,t) + w(x,t), \quad V_\Sigma := \sum_{i=1}^{n} V_i + h(n). \tag{2.10}$$

and assume that the remainder w is transversal to the neutral modes of all kinks, i.e. that

$$\langle w, \psi_i \rangle = 0 \quad \text{for all } t \text{ and all } i = 1, 2, \cdots, n, \tag{2.11}$$

which are *exactly* the orthogonality conditions (2.5) used in the standard scheme. Inserting (2.10) into (1.1) and using that

$$\partial_t V_i = \partial_{xx} V_i + f(V_i) - d_i' \varphi_i, \quad \text{for all } i = 1, 2, \cdots, n, \tag{2.12}$$

we obtain

$$w_t - w_{xx} = \sum_{i=1}^{n} d_i' \varphi_i + f(V_\Sigma + w) - \sum_{i=1}^{n} f(V_i). \tag{2.13}$$

We now carry out a projection onto the neutral Eigenspace which is achieved by multiplying (2.13) with the co-kernel elements ψ_i. To derive equations for $d_i(t)$, we note that due to (2.9) and (2.11),

$$\langle w_t - w_{xx}, \psi_i \rangle = \frac{d}{dt} \langle w, \psi_i \rangle + \langle -\partial_t \psi_i - \partial_{xx} \psi_i, w \rangle = \langle f'(V_i) w, \psi_i \rangle - d_i' \langle w, \partial_x \psi_i \rangle. \tag{2.14}$$

Thus, taking a scalar product of (2.13) with ψ_k, we get the desired system of ODEs

$$\sum_{i=1}^{n} d_i' \langle \varphi_i, \psi_k \rangle + d_k' \langle w, \partial_x \psi_k \rangle = - \left\langle f(V_\Sigma + w) - f'(V_k) w - \sum_{i=1}^{n} f(V_i), \psi_k \right\rangle. \tag{2.15}$$

Note that this system is not resolved with respect to $d'(t) := (d_1'(t), \cdots, d_n'(t))$ and a priori may be ill posed. However, that is not the case when the kinks are well-separated and w is small enough. Indeed, the matrix

$$G(d, w) := \left[\langle \varphi_i, \psi_j \rangle - \delta_{ij} \langle w, \partial_{x_i} \psi_j \rangle \right]_{i,j=1}^{n}, \tag{2.16}$$

in the left-hand side of (2.15) coincides with the Jacobi matrix (2.6) and similarly the matrix is close to the identity if the kinks are well-separated. On the other hand, the matrix $G(d, w)$ may become very small or even singular if some distances between kinks become small which indicates that the projection method is no longer applicable. However, this does yield a sensible condition to stop the simulation i.e., when the condition number of the $G(d, w)$ matrix is large or the distance between any two fronts is less than a certain tolerance. In our simulations we choose to stop the simulation when the distance between any two kinks is $d^{\lim} = 2$. We will investigate this condition further in §3.

To initialise (2.14)-(2.15), we start with a given number n of fronts and set $w \equiv 0$. Evolving (2.14)-(2.15), we find that the fronts either move away from each other, or approach one another. In order to compute through collisions, we monitor the distance between each front and stop evolving (2.14)-(2.15) when any two fronts reach a separation distance of $d^{\lim}$.

Namely, without loss of generality, we may assume that the separation distance is achieved at time moment $t = T_{lim}$ between nth and $n-1$th front and the rest of the fronts remain well-separated (the non-generic case when more than two kinks achieve the collision distance simultaneously is treated analogously):

$$|D_n(T_{lim}) - D_{n-1}(T_{lim})| \approx d_{lim}, \quad |D_{i+1}(T_{lim}) - D_i(T_{lim})| \gg d_{lim}, \quad i = 1, \cdots, n-1.$$

Then, we replace the "old" n-component multi-kink structure

$$u^{old} = u(T_{lim}, x) = \sum_{i=1}^{n} V((-1)^i (x - D_i^{old})) + h(n) + w^{old} := V_\Sigma^{old} + w^{old},$$

by the "new" $(n-2)$-component structure

$$u^{new} = \sum_{i=1}^{n-2} V((-1)^i (x - D_i^{new})) + h(n-2) + w^{new} := V_\Sigma^{new} + w^{new},$$

where the new kink locations D_i^{new} and the new remainder function w^{new} is found from the natural compatibility conditions

$$u^{old} = u^{new}, \quad \langle w^{new}, \psi(x - D_j^{new}) \rangle = 0, \quad j = 1, \cdots, n-2.$$

These are natural conditions to compose since they guarantee that the new update system maintains the orthogonality conditions as stated in (2.5). Therefore one can then define $w^{new} = V_\Sigma^{old} - V_\Sigma^{new} + w^{old}$ and re-write these equations in the form

$$\begin{aligned}\left\langle \sum_{i=1}^{n-2} V((-1)^i(x - D_i^{old})) \right. &- \left. V((-1)^i(x - D_i^{new})), \psi(x - D_j^{new}) \right\rangle + \\ + \left\langle w^{old}, \psi(x - D_j^{new}) - \psi(x - D_j^{old}) \right\rangle &= -\left\langle \sum_{i=n-1}^{n} V((-1)^i(x - D_i^{old})), \psi(x - D_j^{new}) \right\rangle, \quad j = 1, \cdots, n-2.\end{aligned}$$

Here we have implicitly used that $h(n) = h(n-2)$ and the orthogonality conditions for w^{old}. We solve this system of $(n-2)$ equations for the unknowns D_i^{new} via the Newton's method using the "old" kink positions D_i^{old} as the initial approximation. Indeed, the RHS of this equation is a small perturbation since the term $\sum_{i=n-1}^{n} V((-1)^i(x - D_i^{old})$ is localized near the collision point which is assumed to be well-separated from the positions of other kinks and the Jacobi matrix of this system in a small neighborhood of the initial approximation D_i^{old} is close to identity (analogously to (2.5) and (2.6)). Thus, the new kink positions D_i^{new} are uniquely defined and will be close to the old ones D_i^{old}, $i = 1, \cdots, n-2$. When the new kink positions D_i^{new} are derived, the new remainder function w^{new} is computed via

$$w^{new} = u^{old} - \sum_{i=1}^{n-2} V((-1)^i(x - D_i^{new}) - h(n-2).$$

We then evolve the updated projected system (2.14)-(2.15) for the remaining $(n-2)$-kinks with new values D_i^{new} and w^{new} starting from $t = T_{lim}$.

By doing this update to our system, we are able to capture the strong interaction between the colliding fronts while efficiently computing the weak interactions of the remaining well-separated fronts. In the case where we have two fronts left we cannot approximate the collision using PS so we switch to SS. The case of triple or more collisions can be treated analogously.

In order to evolve (2.14)-(2.15), we employ a fourth-order central differences discretisation in space and compute the inner products via Simpson's rule. This yields a large ODE system to evolve and we use the same time stepper as the one used for SS.

As we can see, the above described projection scheme uses in a crucial way the shape of the initial kink (V) as well as its the kernel (φ) and co-kernel (ψ) elements. These functions are known analytically only in some exceptional model cases and usually can be found only numerically. Translates of these functions are needed continuously for the PS scheme and hence one needs to compute these functions in an efficient manner. In order to compute these functions we need to solve to high precision the nonlinear ODE (1.3) (determining V and c) as well as the subsequent linear ODE (1.4) (determining ψ). The kernel element φ can be the found by the numeric differentiation of V.

To this end, we re-write (1.3) and (1.4) as a first order ODE system given by

$$u_\xi = v, \tag{2.17a}$$
$$v_\xi = -f(u) - cv, \tag{2.17b}$$
$$\psi_\xi = \rho, \tag{2.17c}$$
$$\rho_\xi = -f'(u)\psi + c\rho + \lambda\psi, \tag{2.17d}$$

where λ is an Eigenvalue to be solved for and the last two equations solve the adjoint Eigenvalue problem on $\xi \in [-L/2, L/2]$, with projection boundary conditions at $\xi = -L/2$ and $\xi = L/2$ and phase conditions

$$\int_{-L/2}^{L/2} v^{\text{old}}(u - u^{\text{old}}) d\xi = 0, \tag{2.18a}$$
$$\int_{-L/2}^{L/2} v\psi d\xi = 1, \tag{2.18b}$$

where u^{old} is a previously computed front and the last phase condition implements (2.8); see [7]. The first phase condition (2.18)(a) is required so that the computed front solution is unique and centred at the origin (otherwise the front could be arbitrarily translated creating difficultly for any Newton solver since the Jacobian would be singular) while the second phase condition (2.18)(b) is required to fix the arbitrary scaling of the adjoint eigenfunction cf. (1.4). Since we have six equations (2.17)-(2.18), we need six unknowns to solve for. So while we wish to find the $\lambda = 0$ adjoint Eigenfunction, we add λ as an unknown to be solved for and the term $\lambda\psi$ to the last equation of (2.17) to regularise the system; see [7] for details. Since the $\lambda = 0$ adjoint Eigenfunction is isolated and localised, we expect that the solution of (2.17)-(2.18) for $(u, v, \psi, \rho, c, \lambda)$ is unique and well-posed.

We solve the system (2.17)-(2.18) using an orthogonal collocation scheme to discretise (2.17) as described in [4]. The kernel element is v and the co-kernel element is ψ. We initialise the boundary-value problem starting from the case where $f(u, x) = u - u^3$ where there is an explicit solution of the form $(u, \psi) = (\tanh(x/\sqrt{2}), 3\text{sech}^2(x/\sqrt{2})/4)$ and use pseudo-arclength continuation to smoothly change ϵ from zero to yield solutions for the RGL2 and RGL3; see [4] for details on the pseudo-arclength continuation and orthogonal collocation algorithms. The projection boundary conditions yield an error estimate for the domain truncation error of $\mathcal{O}(e^{-2L})$ and are the best possible linear boundary conditions; see [19]. For any simulation of stationary multi-fronts, the computation of a single front need only be done once before the simulation. In the case where we have travelling fronts with different velocities then we should calculate each front and its eigenfunctions separately. For the projection scheme we need to compute the translations of the single front and its eigenfunctions since all the functions are initially computed at the centre of the domain. Therefore, we carry out a piecewise cubic spline interpolation in MATLAB whose error determined by the error of the discretisation of the boundary value problem (2.17). By using this method we can efficiently compute, at each time step, all the required functions at the locations d_i, of each i-*th* front.

3 Results

3.1 Implementation

In order to solve (2.17) and compute a single front, we use the software package AUTO07P [4] with the relative error of the solution set to 5×10^{-12} and NTST=5000, L = 100. For the cubic spline interpolation of the single front to translated fronts, we use the MATLAB routine `interp1`. We choose a spatial discretisation of (2.14)-(2.15) to be $\Delta x = 1 \times 10^{-4}$ such that the absolute error of the inner products and spatial differentiation is $\mathcal{O}(10^{-16})$. To time step SS and PS, we use MATLAB's `ode15s` routine that implements the variable order ODE solver with adaptive time stepping while controlling the relative error to 1×10^{-14}. In order to speed up the time stepping, we provide analytically the Jacobian of the rhs of the ODEs. The routine `ode15s` [23] allows for event detection that allows us to detect when two fronts become close together which we make use of in PS.

In order to carry out the detection of the location of the fronts in the SS scheme, we use MATLAB's `fsolve` routine to solve the nonlinear system (2.5).

All of the results presented in this section have been computed on a machine with the following specifications: Intel(R) Core(TM) Duo CPU E8400 @3.00GHz, 8GB RAM, using Ubuntu 10.04.

3.2 Multi-front solutions of the RGL1 equation

In order to carry out a comparison of the two schemes and investigate their accuracy we start by considering the interaction of two fronts in the RGL1 equation. We first analytically derive the projection scheme and carry out a detailed analysis. We will then use the analysis to compare against the two numerical schemes. To this end, by setting number of fronts $n = 2$ we can derive from the generalised equations (2.13) and (2.15)

the corresponding projected system for two kinks given by

$$d_1' = \frac{\langle R(V) - d_2'\varphi_2, \psi_1\rangle}{\langle w, \psi_1'\rangle - 1} - \Omega(w^2, w^3, V_1, V_2), \tag{3.1a}$$

$$d_2' = \frac{-\langle R(V) - d_1'\varphi_1, \psi_2\rangle}{\langle w, \psi_2'\rangle - 1} + \Omega(w^2, w^3, V_1, V_2), \tag{3.1b}$$

$$\begin{aligned}\frac{\partial w}{\partial t} =& Lw + \left(\frac{\langle R(V) - d_2'\varphi_2, \psi_1\rangle}{\langle w, \psi_1'\rangle - 1} - \Omega(w^2, w^3, V_1, V_2)\right)\varphi_1 \\ &+ \left(\frac{\langle R(V) - d_1'\varphi_1, \psi_2\rangle}{\langle w, \psi_2'\rangle - 1} + \Omega(w^2, w^3, V_1, V_2)\right)\varphi_2 \\ &+ 3\frac{(V_1 - V_2)e^{\frac{d_1-d_2}{\sqrt{2}}}}{\cosh\left(\frac{x-d_1}{\sqrt{2}}\right)\cosh\left(\frac{x-d_2}{\sqrt{2}}\right)} - 3V_1w^2 + 3V_2w^2 + 3w^2 - w^3,\end{aligned} \tag{3.1c}$$

where

$$V_i = \tanh\left(\frac{x-d_i}{\sqrt{2}}\right), \quad L = \partial_{xx} + I + f'(V_1 + V_2), \quad \Omega(w^2, w^3, V_1, V_2) = \frac{\langle 3V_1w^2 - 3V_2w^2 - 3w^2 + w^3, \psi_i\rangle}{\langle w, \psi_i'\rangle - 1},$$

$$R(V) = \frac{3e^{\frac{d_1-d_2}{\sqrt{2}}}(V_1 - V_2)}{\cosh\left(\frac{x-d_1}{\sqrt{2}}\right)\cosh\left(\frac{x-d_2}{\sqrt{2}}\right)},$$

and $\psi_i = 3\text{sech}^2((x - d_i/\sqrt{2})/4$.

A leading order approximation for how the two fronts interact can be found by assuming that the remainder function w is zero i.e., the solution is just the two fronts. Setting $w = 0$, the equations for the translations of the two fronts simplify to

$$d_1' = \frac{\langle R(V), \psi_1\rangle - \langle \varphi_2, \psi_1\rangle\langle R(V), \psi_2\rangle}{1 + \langle \varphi_1, \psi_2\rangle\langle \varphi_2, \psi_1\rangle}, \tag{3.2a}$$

$$d_2' = \frac{-\langle R(V), \psi_2\rangle + \langle \varphi_1, \psi_2\rangle\langle R(V), \psi_1\rangle}{1 + \langle \varphi_1, \psi_2\rangle\langle \varphi_2, \psi_1\rangle}, \tag{3.2b}$$

where

$$\langle R(V), \psi_i\rangle = (-1)^{i+1}\frac{6\sqrt{2}\left(e^{3d(t)\sqrt{2}} + (9 - 6b\sqrt{2})e^{2d(t)\sqrt{2}} - (9 + 6b\sqrt{2})e^{d(t)\sqrt{2}} - 1\right)}{-e^{4d(t)\sqrt{2}} + 4e^{3d(t)\sqrt{2}} - 6e^{2d(t)\sqrt{2}} + 4e^{d(t)\sqrt{2}} - 1},$$

$$\langle \varphi_1, \psi_2\rangle = \langle \varphi_2, \psi_1\rangle = -\frac{6\sqrt{2}e^{d(t)\sqrt{2}}\left(e^{d(t)\sqrt{2}}(2 - d(t)\sqrt{2}) - d(t)\sqrt{2}\right)}{3e^{d(t)\sqrt{2}} - 3e^{2d(t)\sqrt{2}} + e^{3d(t)\sqrt{2}} - 1}.$$

Taking the leading order terms on the right hand side of (3.2) one can find the approximation for $d(t) = |d_1(t) - d_2(t)|$ given by

$$d(t) \approx -\frac{1}{\sqrt{2}}\log\left(6t + e^{\sqrt{2}d(0)}\right), \tag{3.3}$$

where $d(0)$ is the initial separation of the fronts. The error of this approximation decays exponentially as the separation distance $d(t)$ increases. Crucially, this estimate tells us that two kinks are attracted to each other and should eventually come together for some finite T. Furthermore, in cases of multiple kinks, if a pair of fronts is well separated from the other kinks, then we still have similar behaviour due to the fact that these weak interactions do not affect leading order terms.

In Figure 2 (a), we show how the distance between the two kinks evolves leading to a collision and annihilation. The PS scheme (3.1) is evolved till the kinks have a separation distance of 2 and then we switch to SS scheme in order to compute the strong interaction and collision. We also plot the analytical approximation (3.3) alongside for comparison. We see that initially the two fronts slowly become attracted to each other and as they become closer together the two fronts move quicker. Eventually, the two fronts collide at $t \approx 415$ and annihilate each other. We note that when two fronts collide, we always have an exponentially decaying trace that takes infinite time for it to dissipate. Therefore, we define collision time as the the time point where

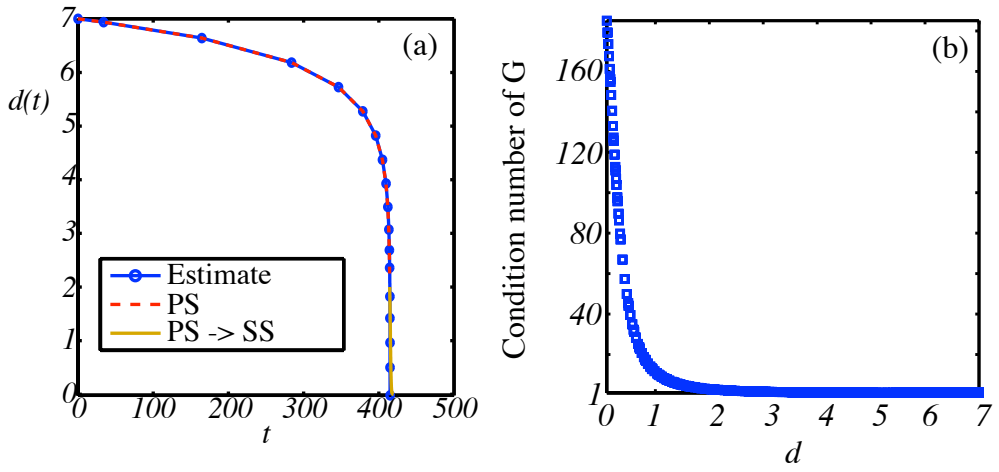

Figure 2: ***(a)*** *Comparison of analytic estimate (3.3) with numerical results of the distance between two well separated kinks with $d(0) = 7$. The numerical results are split into two segments, the projected system (PS) and the standard time stepping scheme (SS) data.* ***(b)*** *The condition number of the matrix $G(d, w)$ i.e., $\|G(d, w)^{-1}\|_2 \|G(d, w)\|_2$, as the distance between the two kinks decreases. We see that for $d(t) < 1$, the condition number of G rapidly increases.*

the decaying trace has machine accuracy order, i.e $\mathcal{O}(10^{-16})$. In Figure 2 (b) we plot the condition number of the matrix $G(d, w)$, $\|G(d, w)^{-1}\|_2 \|G(d, w)\|_2$ where $\|\cdot\|_2$ is the matrix 2-norm, as the distance between the two kinks decreases. We see that as the separation distance decreases below 1, the condition number rapidly increases suggesting that the PS scheme breaks-down in this region. Hence, stopping the PS scheme at a distance $d(t_{\text{lim}}) = 2$ yields a sensible criteria for transitioning to the SS scheme and propagating the fronts till collision and annihilation.

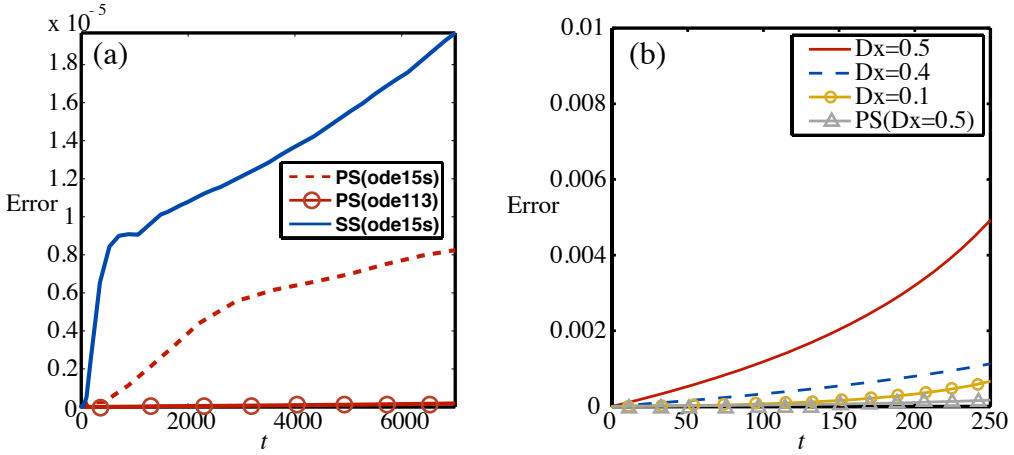

Figure 3: ***(a)*** *Comparison of the two schemes with different solvers for $d(0) = 10$ with $\Delta x = 0.005$* ***(b)*** *Convergence of SS scheme and comparison of schemes regarding space step Δx for initial conditions $d(0) = 7$.*

In order to test the accuracy of the schemes, we solve (3.2) using MATLAB's high accuracy solver `ode113` and define the error to be the absolute value of the difference between $d(t)$ and the SS/PS scheme (where one carries out numerical integration for the inner products) and the `ode15s` scheme. In Figure 3 (a), we show how the error evolves over time starting for $d(0) = 10$ with $\Delta x = 0.005, Lx = 50$. We see that although the error increases over time for both numerical schemes, SS appears to have a significantly larger error whereas the PS scheme remains more accurate over time. We note that the solver `ode113` is feasible only for special cases where the system does not involve a stiff PDE. We see that the the PS scheme remains accurate even for very large spatial steps where as for similar spatial step sizes the SS scheme performs very poorly; see Figure 3 (b). This highlights the robustness of the PS scheme compared to the SS scheme and also that for long simulations one might expect the SS scheme to be slower than the PS scheme.

$d(0)$	Scheme	Δx	Δt	Error	Comp. Time
7	SS	0.01	< 0.1	8.41e-4	3.54
7	PS	0.5	Adapt.	9.17e-5	3.21
10	SS	0.01	< 0.1	5.33e-8	3.53
10	PS	0.01	Adapt.	3.56e-9	2.79
15	SS	0.01	< 0.1	8.7e-8	3.57
15	SS	0.01	< 0.01	8.68e-8	50.53
15	PS	0.01	Adapt.	1.53-11	1.93

Table 1: *Computational time and error comparison of the SS and PS schemes both evaluated at* $t = 200$ *for three different initial conditions where* $d(0) = 7, d(0) = 10$ *and* $d(0) = 15$.

In Table 1, we show the computational wall time taken and the error at $t = 200$ with respect to evolving (3.2) with MATLAB's `ode15s` solver. We find for the SS scheme, one needs to stipulate a maximum time step in order to avoid large errors. Since the SS and PS schemes compute different things we show the computational time taken to compute the full solution $u(x,t)$ of the PDE. We find that for these short simulations, the PS scheme outperforms SS scheme in all cases by providing a more accurate estimate and taking less computational time. In fact the computational times are only close in the case where we have the strongest interaction between the two fronts. Considering weak interacting fronts (e.g. $d(0) = 10,\ d(0) = 15$), the PS scheme excels by making full use of the adaptive time stepping. For very long simulations requiring very tight error tolerances we expect the PS scheme to out perform the SS scheme significantly due to the later requiring to solve a larger set of ODEs and the small time step.

We find that the adaptive time stepper, `ode15s`, for the PS scheme can take large time steps due to the fact that remainder function $w(x,t)$ remains small and evolves slowly for weak interacting fronts. The evolution of $w(x,t)$ is slaved to the location variables $d_i(t)$ which evolve slowly for well separated fronts. However, in cases where fronts become strong interacting remainder function $w(x,t)$ grows in time since location variables $d_i(t)$ evolve much faster and the time-stepper has to take smaller time steps.

We will now investigate various multi-front solutions of the RGL using the PS scheme. In almost all cases we observe that fronts annihilate each other in pairs. However, it is possible to create a degenerate case where three fronts collide at the same point with one left after the collision provided the fronts are initial equi-spaced. Setting the initial front locations to be $d_1(0) = a, d_2(0) = 0$ and $d_3(0) = -a$ for some positive constant a, we find that the projected system (2.13) and (2.15) with the number of fronts set to three i.e., $n = 3$, possesses the symmetry $d_1(t) \to -d_3(t)$ and that $d_2'(t) = 0$ for all time. Setting $w = 0$, the equations (2.13) and (2.15) for $n = 3$ to leading order are given by

$$d_1' = -12\sqrt{2}e^{-|d_1|\sqrt{2}} + \mathcal{O}(e^{-2|d_1|\sqrt{2}}). \tag{3.4}$$

Equation (3.4) is identical to the 2-front case since the the third front has distance $2d_1$ (from the first front) and produces only second order corrections to the leading interactions term. The approximation (3.4) provides a good estimate as to how the location of front evolves over time for weak interactions and we see that since the righthand-side of (3.4) is negative to leading order, the variable $d_1(t)$, decreases. Hence, we expect all three fronts to collide at the same point.

In Figure 4 (a), we show the evolution of three fronts equally spaced. For such solutions, one expects the simulations to remain symmetric with the middle front remaining unaffected by the two fronts attracting to it until all three fronts collide together. One has to be careful with setting the point to stop the PS scheme when the fronts become close together as numerical roundoff errors become amplified as the scheme becomes ill-posed. In Figure 4 (b) we plot the condition number of $G(d,w)$ as the distance between the three kinks goes to zero; here $d(t) = |d_3(t) - d_2(t)| = |d_2(t) - d_1(t)|$. We see that for separation distances below 2 the condition number rapidly increases and in fact the matrix G becomes singular at $d(t) \approx 1.2$. Hence, we find that stopping the PS scheme when the distance between the three fronts is 2 works well in this case.

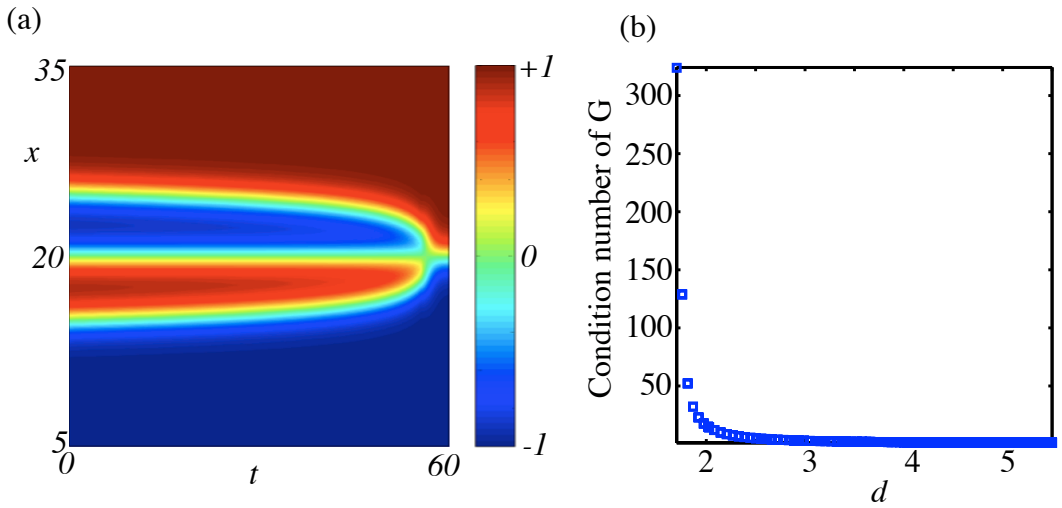

Figure 4: ***(a)*** *Evolution of three equidistant kink solution with initial conditions* $d_1(0) = 15,\ d_2(0) = 20,\ d_3(0) = 25$ *and spatial step* $\Delta x = 0.001$. *At* $t \approx 52$ *all three kinks collide and one kink survives at the end.* ***(b)*** *The condition number of* $G(d, w)$ *i.e,* $\|G(d, w)^{-1}\|_2 \|G(d, w)\|_2$, *verses the separation distance* $d(t) = |d_3(t) - d_2(t)| = |d_2(t) - d_1(t)|$.

Next, we consider six equi-spaced fronts with initial locations $d_1(0) = 15,\ d_2(0) = 20,\ d_3(0) = 25,\ d_4(0) = 30,\ d_5(0) = 35,\ d_6(0) = 40$. In Figure 5 (a) we observe how the six fronts evolve together by using the PS scheme. We see that the four outer fronts have two collisions at $t \approx 33$ before the two remaining fronts annihilate each other at $t \approx 55$. Near the first set of collisions (when the separation distance between the two fronts is two), we see in Figure 5 (b) how the PS process strong interacting fronts using remainder function $w(x, t)$ which is vital for computing strong interactions. When the separation distance of the kinks reaches 2, the PS scheme is stopped and the corresponding equations of strongly interacting fronts (d_1, d_2, d_5 and d_6) are removed with new initial conditions for d_3, d_4 and w computed. The new initial conditions have a jump that is small in d_3 and d_4 but large in w since it now includes the colliding front pairs (centred at $x = 37.5$ and $x = 17.5$); see Figure 5 (b) showing the jump in the w-function around the first collision at $t \approx 33$. From there we track the colliding fronts from the remainder function w plotted in Figure 5 (a) as a dashed red line denoted as *WPDE*. We now simulate the reduced PS system until the next collision. With this approach we are able to accurately capture the weak interactions of the multi-fronts and the colliding fronts.

In Figure 6 (a) we show the simulation of five equi-spaced fronts where we observe the middle front survives after the other two pairs collide and annihilate. Figure 6 (b) presents the evolution of nine fronts with not equi-spaced. In this case we find the front closest to each other attract and annihilate each other due to them having the largest interaction forces.

3.3 Multi-front solutions of RGL2 equation

We will now look at how the projection scheme can apply to the case where a single front is travelling in the RGL2 equation. The RGL2 equation possesses explicit travelling front solutions of the form

$$V(x - ct - d(t)) = \tanh\left(\frac{x - ct - d(t)}{\sqrt{2}}\right),$$

where $c = \pm\epsilon\sqrt{2}$. Depending on the initial direction of the travelling fronts, we observe either collision of repulsion. In Figure 7 (a) we present the simulation of two travelling fronts of the RGL2 equation with the fronts initially located at $d_1(0) = 15,\ d_2(0) = 25$ and $\varepsilon = 0.5$. Choosing travelling fronts that move towards each other, we expect a collision at $t = 10\sqrt{2}$ and we observe a collision at approximately this value since the interaction terms are significantly weaker than the travelling speed of the fronts.

The effect of the perturbation term, $\varepsilon(u^2 - 1)$, on the front interaction can be approximated when $\varepsilon \ll 1$.

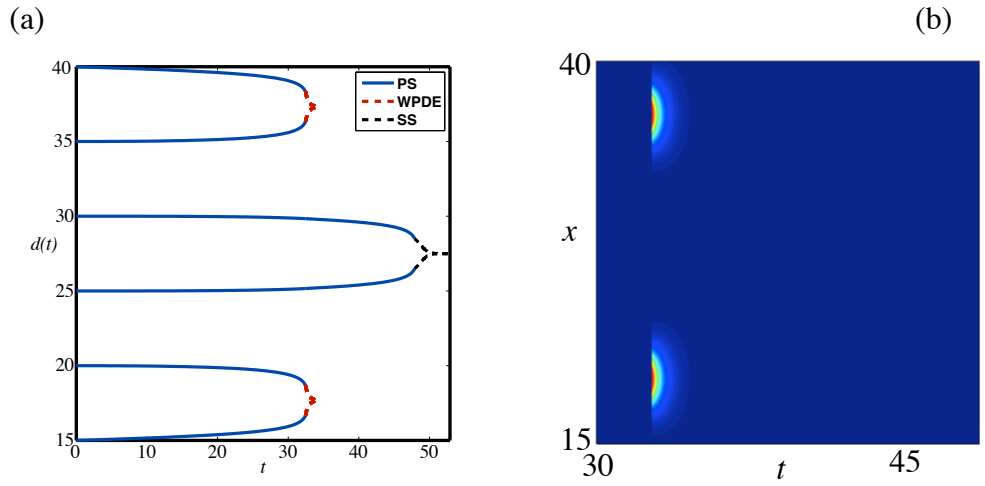

Figure 5: ***(a)*** *Evolution of translation variables for 6 equidistant kinks with initial conditions* $d_1(0) = 15$, $d_2(0) = 20$, $d_3(0) = 25$, $d_4(0) = 30$, $d_5(0) = 35$, $d_6(0) = 40$. *We see that the two outer pairs (including first, second, fifth and sixth fronts) collide at the same time* ($t \approx 33$). *The middle two kinks survive and collide at a later time. Near where the first collisions occur at* $t \approx 33$, *the PS stops and updates the system by removing the corresponding ODEs for the colliding fronts* (d_1', d_2', d_5' *and* d_6') *and by using new initial conditions for* d_3, d_4 *and* w, *we continue the numerics using a new well-posed system. We then track the colliding fronts from* w *using* (2.5), *plotted in dash red denoted at WPDE. For the final collision, we switch from the PS scheme to the SS scheme and track the fronts in the same manner, shown as dashed black. Panel* ***(b)*** *shows the jump observed as a result of the new initial conditions for remainder function* $w(x,t)$ *near the first collision at* $t \approx 33$ *where we stop PS. We see that before the collision* w *is approximately zero until the distance between the fronts reaches* 2. *When the separation distance between the first & second, and fifth & sixth fronts reaches* 2, *PS scheme is stopped and and new PS system is computed with new initial conditions. At this point we see a sudden jump in the* w*-function centred at the locations of the colliding kinks. Re-starting the new PS system, we see that* w *quickly decays to zero.*

Setting $w = 0$, we find the leading order system to be,

$$d_1' - \langle d_2' \varphi_2, \psi_1 \rangle = +I_1 + \varepsilon P_1, \tag{3.5}$$

$$d_2' - \langle d_1' \varphi_1, \psi_2 \rangle = -I_2 + \varepsilon P_2, \tag{3.6}$$

where $f(u) = u - u^3$, $I_i = \langle f(V_1 - V_2 - 1) - f(V_1) + f(V_2), \psi_i \rangle$ are the terms due to the front interacting via their tails and $P_i = \langle (V_1 - V_2 - 1)^2 - 1, \psi_i \rangle$ are the terms due the perturbation term $\varepsilon(u^2 - 1)$. Setting $\varepsilon = 0$, we find that the fronts interact exactly as before for the RGL1. Since $I_i = \mathcal{O}(e^{-\sqrt{2}|d_1 - d_2|})$ and $P_i = \mathcal{O}(1)$, then the size of ε will determine whether the dynamics are mostly governed by the front interaction terms or the perturbation terms. In particular, if $|\varepsilon| < \mathcal{O}(e^{-\sqrt{2}|d_1 - d_2|})$, then the fronts will behave qualitatively similar to when $\varepsilon = 0$ i.e., the fronts will collide and annihilate each other with only difference being that collision point of the fronts may be slightly shifted. When $|\varepsilon| > \mathcal{O}(e^{-\sqrt{2}|d_1 - d_2|})$, the perturbation terms P_i dominate and depending on the sign of ε one can observe fronts moving away from each other $\varepsilon < 0$ or colliding $\varepsilon > 0$.

For $|\varepsilon| > 1$, one of two $u = \pm 1$ (depending on ε sign) equilibriums becomes unstable and analysis on the dynamics becomes challenging. In Figure 7 (b), we show what happens to six fronts for $\varepsilon = 5$ with initial locations of $d_1(0) = 10$, $d_2(0) = 50$, $d_3(0) = 70$, $d_4(0) = 90$, $d_5(0) = 110$, $d_6(0) = 140$ and wave speeds $\pm 5\sqrt{2}$. In this case, we observe that the fronts behave in a very similar fashion as for $\varepsilon < 1$.

3.4 Multi-fronts solutions of the RGL3 equation

We will now look at the case where we have spatial inhomogeneities in the PDE e.g. the RGL3 equation. For the RGL3 equation we expect to see bound states occurring due to the small periodic in-homogeneity if ε and the initial separation distances of the fronts are chosen correctly. Setting $w = 0$, we find the leading

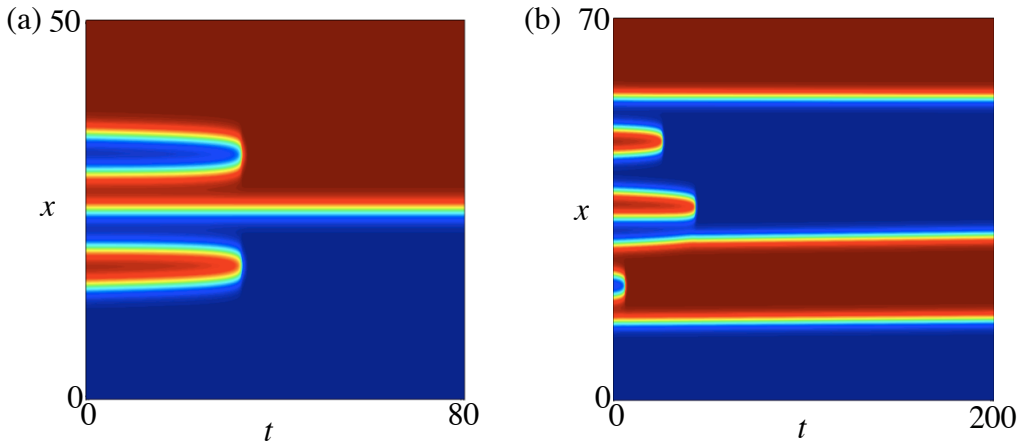

Figure 6: *Evolution of multi-kinks* ***(a)*** *We consider 5 kink equidistant solution with initial conditions* $d_1(0) = 15,\ d_2(0) = 20,\ d_3(0) = 25,\ d_4(0) = 30,\ d_5(0) = 35,$ *and* $\Delta x = 0.001$. *The collision of the two pairs leaves only one kink surviving at the end.* ***(b)*** *We consider 9 kink equidistant solution with initial conditions* $d_1(0) = 15,\ d_2(0) = 20,\ d_3(0) = 24,\ d_4(0) = 30,\ d_5(0) = 35,\ d_6(0) = 40,\ d_7(0) = 47,\ d_8(0) = 52,\ d_9(0) = 59,$ *and* $\Delta x = 0.001$. *Kinks detect which kink is closer to them and move towards it.*

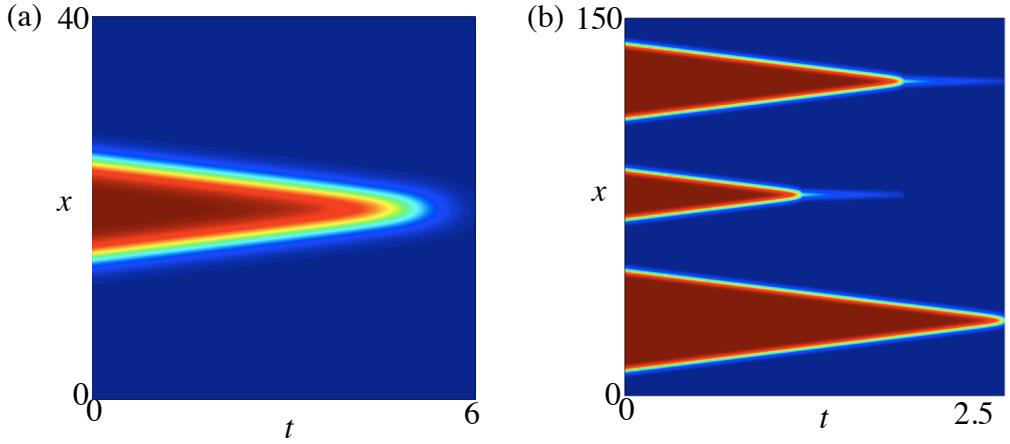

Figure 7: ***(a)*** *Two traveling fronts, with initial conditions* $d_1(0) = 15,\ d_2(0) = 25,\ \varepsilon = 0.5$ *and* $\Delta x = 0.001$. *Since we are considering a kink-antikink solution kinks move towards each other and collide with velocity* $|c| \approx 0.5\sqrt{2}$ ***(b)*** *Six high velocity travelling fronts with initial conditions* $d_1(0) = 10,\ d_2(0) = 50,\ d_3(0) = 70,\ d_4(0) = 90,\ d_5(0) = 110,\ d_6(0) = 140,\ \varepsilon = 5$ *and* $\Delta x = 0.001$.

order ODE system describing location of the two fronts for perturbation function $r(x) = \varepsilon\cos(x-\alpha)$ to be

$$d_1' - \langle d_2'\varphi_2, \psi_1\rangle = +I_1 + \varepsilon P_1, \tag{3.7}$$
$$d_2' - \langle d_1'\varphi_1, \psi_2\rangle = -I_2 - \varepsilon P_2 \tag{3.8}$$

where

$$I_i = \langle f(V_1 - V_2 - 1) - f(V_1) + f(V_2), \psi_i\rangle, \qquad \text{and,} \qquad P_i = \langle \cos(x-\alpha), \psi_i\rangle,$$

$f(u) = u - u^3$ and α is a real constant. Here the terms I_i are due to the fronts interacting via their tails and the P_i terms are due to the fronts interacting with the spatial inhomogeneity. As in the RGL2 case, depending on the sign and size of ε one will observe different dynamics since $I_i = \mathcal{O}(e^{-\sqrt{2}|d_1-d_2|})$ and $P_i = \mathcal{O}(1)$. When $\varepsilon < \mathcal{O}(e^{-\sqrt{2}|d_1-d_2|})$, perturbation terms P_i are not large enough to impact the dynamics of the two fronts and they will collide and annihilate each other similar to the dynamics of RGL1 equation. The small terms introduced will shift slightly the collision point for the fronts but annihilation is inevitable once again. If $\varepsilon > \mathcal{O}(e^{-\sqrt{2}|d_1-d_2|})$, then the perturbation terms dominate the dynamics and one will observe the fronts converging to bound states.

In Figure 8 (b) we show the evolution of two fronts located at $d_1(0) = 25$ and $d_2(0) = 30$. We have chosen $\varepsilon = 0.05$ and $r(x) = \cos((x-25)/2)$ in order for the perturbation term $\varepsilon r(x)$ to have slightly higher order than interaction terms $|d_1'(0) - d_2'(0)| \approx 0.02$. More specifically, in Figure 8 (a) we can see how the inhomogeneity $r(x)$ acts differently on the two fronts such that for the front centred at $x = 25$, $r(25) \approx 1$ and for front located at $x = 30$ where $r(30) \approx -1$, preventing the two fronts from colliding and annihilating one another. Moreover in Figure 8 (b) one can see that the fronts initially translate but very quickly converge to a single pulse at $t \approx 100$. Depending on the location of the fronts we can observe a variety of behaviors such as annihilation; see Figure 9 where we simulate six fronts located at $d_1(0) = 25$, $d_2(0) = 30$, $d_3(0) = 36$, $d_4(0) = 40$, $d_5(0) = 45$, $d_6(0) = 50$. We can see in Figure 9 the two outer pairs with separation distance equal 5 converge to bound states whereas the middle pair of fronts (d_3, d_4) with separation distance 4 collide and annihilate. The behavior seen in 9 occurs due to strong interaction of the fronts producing higher order terms that cannot be canceled by the perturbation function.

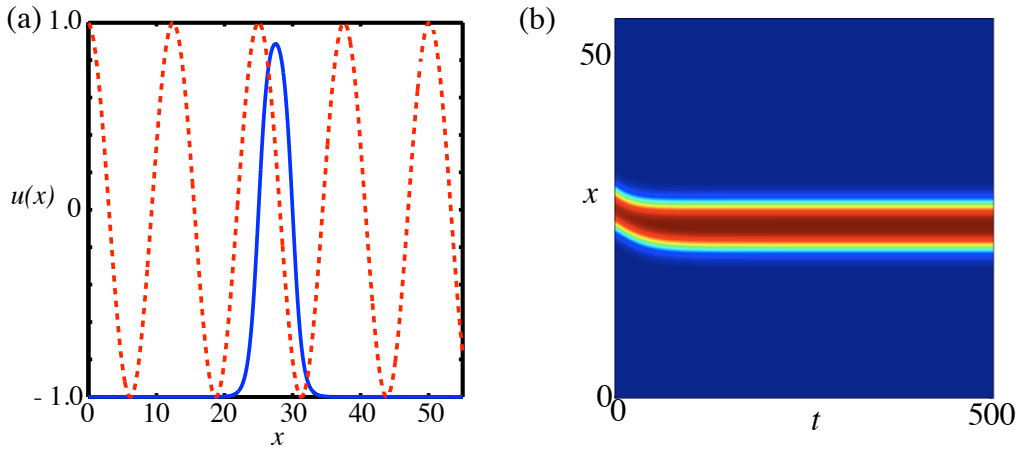

Figure 8: ***(a)*** *A plot of the perturbation* $r(x) = 0.05\cos\left(\frac{x-25}{2}\right)$ *and the final bound state with* $\Delta x = 0.001$. ***(b)*** *Evolution of two kinks over time; after some initial transient the kinks converge to bound states.*

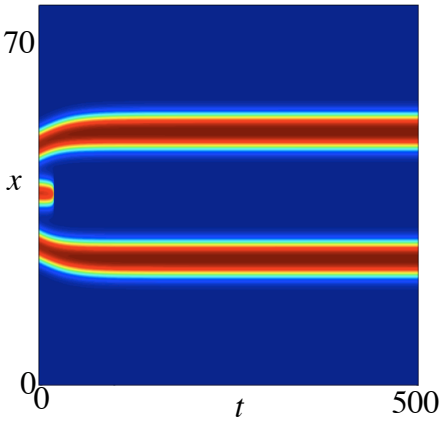

Figure 9: *Evolution of six kinks over time with initial conditions* $r(x) = cos\left(\frac{x-25}{2}\right)$, $d_1(0) = 25$, $d_2(0) = 30$, $d_3(0) = 36$, $d_4(0) = 40$, $d_5(0) = 45$, $d_6(0) = 50$, $\varepsilon = 0.05$ *and* $\Delta x = 0.001$. *We can see two pairs of kinks converging, however the pair that has interaction terms* $d'(0) = d_4'(0) - d_3'(0) > O(\varepsilon r(x))$ *stays unaffected by the perturbation and the two kinks collide.*

4 Conclusion

In this paper, we have presented a novel numerical method for simulating multi-fronts in RGL equations based on the global centre-manifold reduction for multi-localised structures. The addition of a remainder function in the ansatz allows us to accurately compute through collisions of fronts via a careful detection of the separation distances of the fronts, halting the computation and initialising a new PS system with specially chosen initial conditions. This scheme is found to be significantly more robust and efficient than evolving a standard finite-difference discretisation of the RGL equation. In particular, for coarse meshes the PS scheme significantly out performs SS scheme by explicitly capturing the interaction terms. The main reason for the robustness of the scheme is that a single front and its neutral Eigenfunction is accurately computed once and the accuracy of the time-stepping is governed by the accuracy of this single front computation. Since the expensive computation of a single front is done only once and the computation of the interaction terms being fast (due to the inner products having significantly better error terms than derivative terms), the time-stepping scheme becomes a very efficient method for evolving multi-fronts.

We have tested the PS scheme on three different RGL type equations in order to explore a variety of different multi-front states. We started by presenting simulations of two-, three- and many multi-fronts interact with each other in the RGL1 equation. We found in all cases for the RGL1 equation, fronts attract one another resulting in collisions and annihilations of the fronts. In particular, we showed that the PS scheme is sufficiently robust to capture the collision of three equi-spaced fronts that collide together simultaneously. The PS scheme can be easily extended to cope with the case where an individual front is travelling and inhomogeneous terms are added to the RGL equation.

Let us now discuss the generality and extensions of the PS scheme. The centre-manifold theory of Zelik & Mielke [27] has been proved for a general parabolic PDE system with a strongly elliptic differential operator involving general weakly interacting localised structures in several space dimensions. Hence, the numerical PS scheme presented in this paper extends to a large class of problems. In particular, one can study the interacting of localised pulses on the plane that are elliptical, or hexagon patches. An open problem is the development of a centre-manifold theory for weakly interacting localised structures with internal dynamics such as oscillons. Another interesting direction for research is to investigate the interaction of multi-localised structures in Hamiltonian systems where the linearisation of a single localised structure is not normally-hyperbolic.

One of the main advantages of our scheme is the explicit computation of the small interaction terms where we are able to keep control on all the numerical error tolerances. However, we are still limited by machine precision arithmetic in particular the numerical scheme we have implemented is limited to double precision arithmetic i.e., separation distances of order less than $\log(\alpha[1 \times 10^{-16}])$ where α is the linear decay rate to the base state. Another problem with evolving fronts with large separation is that they will move on exponentially large time-scales requiring very fast time-steppers. The problem with machine precision can be easily overcome by using extended or arbitrary precision arithmetic. However, then the development of fast time-steppers becomes extremely important due to the computational cost of computing with such high precision. In order to overcome the exponentially slow time evolution, we suggest that a rescaling in time with the leading order interaction terms e.g. $t = e^{-\alpha d(\tau)}\tau$ where d is the separation distance between two localised structures. This rescaling will lead to a system with order one terms for the ODEs describing the location of the localised structures with a PDE system describing the slow evolution of the perturbation function w. One then needs to develop fast and efficient time-steppers to take advantage of this new fast-slow ODE/PDE system and we leave this for further work. The major advantage of this approach will be that the expensive computation of the single localised state and its neutral eigenfunction has to only be done once and the inner product terms having better error terms than numerical differentiation. Another advantage is that one should be able to break the computation of interacting localised states into three different schemes based on large, middle and short separation distances. For large separation of fronts, one can use the rescaling of time and treat w as slaved to the location of the fronts. For the middle and short

separations, one can use the numerical scheme described in this paper. Hence, one should be able to deal effectively with multi-fronts/pulses from extremely well-separated to colliding.

Another interesting extension is the computation of pulses/fronts after collision that do not lead to annihilation. We anticipate that any collision of localised states should at most generate finitely many new localised states and our numerical scheme should be able to capture the nucleation of these new states. One then needs a good detection mechanism to halt the simulation when the localised states become sufficiently well separated in order to re-compute the projected system and efficiently capture the weak interaction terms. We leave the investigation of this process and development of the numerical algorithm for further work.

In conclusion, we have presented a numerical approach for evolving multi-pulses/fronts that has the potential to simulate extremely well separated fronts or pulses to collision and beyond efficiently and accurately.

References

[1] Nail Akhmediev and Adrian Ankiewicz. *Solitons: nonlinear pulses and beams*. Vol. 4. London: Chapman & Hall, 1997.

[2] U. M. Ascher and R. D. Russell, editors. *Numerical boundary value ODEs*, volume 5 of *Progress in Scientific Computing*, Boston, MA, 1985. Birkhäuser Boston Inc.

[3] M. Bär, M. Eiswirth, H.-H. Rotermund, and G. Ertl. Solitary-wave phenomena in an excitable surface reaction. *Phys. Rev. Lett.*, 69:945–948, Aug 1992.

[4] E. J. Doedel, R. C. Paffenroth, A. R. Champneys, T. F. Fairgrieve, Yu. A. Kuznetsov, B. E. Oldeman, and B. Sandstede. Auto07p: Continuation and bifurcation software for ordinary differential equations. Technical report, Concordia University, Department of Computer Science, Montreal, Canada, 2007. Available via http://www.dynamicalsystems.org/.

[5] J.-P. Eckmann and J. Rougemont. Coarsening by Ginzburg-Landau dynamics. *Comm. Math. Phys.*, 199(2):441–470, 1998.

[6] Shin-Ichiro Ei. The motion of weakly interacting pulses in reaction-diffusion systems. *J. Dynam. Differential Equations*, 14(1):85–137, 2002.

[7] Mark J. Friedman and Eusebius J. Doedel. Numerical computation and continuation of invariant manifolds connecting fixed points. *SIAM J. Numer. Anal.*, 28(3):789–808, 1991.

[8] K. A. Gorshkov, L. A. Ostrovsky, V. V. Papko, and A. S. Pikovsky. On the existence of stationary multisolitons. *Phys. Lett. A*, 74(3-4):177–179, 1979.

[9] Daniel Henry. *Geometric theory of semilinear parabolic equations*, volume 840 of *Lecture Notes in Mathematics*. Springer-Verlag, Berlin-New York, 1981.

[10] David Kahaner, Cleve Moler, and Stephen Nash. Numerical methods and software. *Englewood Cliffs: Prentice Hall, 1989*, 1, 1989.

[11] John H. Merkin, Valery Petrov, Stephen K. Scott, and Kenneth Showalter. Wave-induced chemical chaos. *Phys. Rev. Lett.*, 76:546–549, Jan 1996.

[12] J. D. Murray. *Mathematical biology. I*, volume 17 of *Interdisciplinary Applied Mathematics*. Springer-Verlag, New York, third edition, 2002. An introduction.

[13] Yasumasa Nishiura, Takashi Teramoto, and Kei Ueda. Scattering of traveling spots in dissipative systems. *Chaos: An Interdisciplinary Journal of Nonlinear Science*, 15(4):047509, 2005.

[14] Yasumasa Nishiura, Takashi Teramoto, and Kei-Ichi Ueda. Scattering and separators in dissipative systems. *Phys. Rev. E*, 67:056210, May 2003.

[15] Yasumasa Nishiura and Daishin Ueyama. A skeleton structure of self-replicating dynamics. *Physica D: Nonlinear Phenomena*, 130(1):73–104, 1999.

[16] Bart E. Oldeman, Alan R. Champneys, and Bernd Krauskopf. Homoclinic branch switching: a numerical implementation of Lin's method. *Internat. J. Bifur. Chaos Appl. Sci. Engrg.*, 13(10):2977–2999, 2003.

[17] J. Rougemont. Dynamics of kinks in the ginzburg-landau equation: approach to a metastable shape and collapse of embedded pairs of kinks. *Nonlinearity*, 12(3):539–554, 1999.

[18] B. Sandstede, C. K. R. T. Jones, and J. C. Alexander. Existence and stability of N-pulses on optical fibers with phase-sensitive amplifiers. *Phys. D*, 106(1-2):167–206, 1997.

[19] Björn Sandstede. Convergence estimates for the numerical approximation of homoclinic solutions. *IMA J. Numer. Anal.*, 17(3):437–462, 1997.

[20] Bjorn Sandstede. Stability of travelling waves. *Handbook of dynamical systems, North-Holland, Amsterdam*, 2:983–1055, 2002.

[21] Arnd Scheel and J. Douglas Wright. Colliding dissipative pulses—the shooting manifold. *J. Differential Equations*, 245(1):59–79, 2008.

[22] L. F. Shampine. *Numerical Solution of Ordinary Differential Equations*. Chapman & Hall, New York., 1994.

[23] Lawrence F. Shampine and Mark W. Reichelt. The MATLAB ODE suite. *SIAM J. Sci. Comput.*, 18(1):1–22, 1997. Dedicated to C. William Gear on the occasion of his 60th birthday.

[24] G. D. Smith. *Numerical solution of partial differential equations*. Clarendon Press, Oxford, 2nd edition edition, 1978.

[25] Aizik I. Volpert, Vitaly A. Volpert, and Vladimir A. Volpert. *Traveling wave solutions of parabolic systems*, volume 140 of *Translations of Mathematical Monographs*. American Mathematical Society, Providence, RI, 1994. Translated from the Russian manuscript by James F. Heyda.

[26] A. C. Yew, A. R. Champneys, and P. J. McKenna. Multiple solitary waves due to second-harmonic generation in quadratic media. *J. Nonlinear Sci.*, 9(1):33–52, 1999.

[27] Sergey Zelik and Alexander Mielke. Multi-pulse evolution and space-time chaos in dissipative systems. *Mem. Amer. Math. Soc.*, 198(925):vi+97, 2009.